Theor Chem Acc (2000) 104:445–454
DOI 10.1007/s002140000164

Theoretical
Chemistry Accounts

Regular article

An investigation of basis set effects in the characterization of electron – atom scattering resonances using the dilated electron propagator method

Arun Venkatnathan[1], **Manoj K. Mishra**[1], **Hans Jørgen Aa. Jensen**[2]

[1]Department of Chemistry, Indian Institute of Technology, Bombay, Powai, Mumbai 400 076, India
[2]Department of Chemistry, University of Southern Denmark – Odense University, 5230 Odense M, Denmark

Received: 3 January 2000 / Accepted: 5 March 2000 / Published online: 21 June 2000

Abstract. The effects of basis set variations on resonance attributes are investigated using systematically augmented basis sets by correlating the resulting changes in resonance energy and width with the alterations induced in the radial probability density profile of the resonant orbital. Applications to ^{2}P Be$^-$ and ^{2}P Mg$^-$ shape resonances reveal that basis sets capable of describing both electron density accumulation near the target nucleus to facilitate resonance formation and sufficiently large electron density away from the target nucleus to provide for its decay are necessary for effective characterization of these resonances. A comparison of radial probability density profiles from the bivariational self-consistent field, the second-order, the diagonal two particle–one hole Tamm–Dancoff approximation and quasiparticle decouplings reveals that relaxation effects dominate in resonance formation.

Key words: Electron scattering – Shape resonance – Electron propagator – Complex scaling – Bivariational self-consistent held

1 Introduction

The electron propagator technique [1, 2] has emerged as a potent tool for the correlated treatment of electronic structure [3–7]. The complex scaled [8, 9] electron propagator [10–12], where all the electronic coordinates of the Hamiltonian have been scaled by a complex scale factor ($\eta = \alpha e^{i\theta}$) has emerged as an effective technique for investigation of shape resonances in electron–atom and electron–molecule scattering [13–15]. The biorthogonal dilated electron propagator [14] is based on an underlying bivariational self-consistent-field (SCF) method [16, 17] which takes full cognizance of the non-Hermiticity of the complex scaled Hamiltonian, while preserving the simple structure of the real electron propagator formalism. Different decouplings of the dilated electron propagator, such as the zeroth-order (Σ^0), the second-order (Σ^2) and the diagonal two particle–one hole Tamm–Dancoff ($\Sigma^{2\text{ph-TDA}}$) approximations and the corresponding quasiparticle decouplings have been implemented and offer effective description of energies and widths of shape resonances of atomic and molecular systems [14, 15].

It has become amply clear from these investigations [14–27] that basis set effects are critical in the characterization of resonances, since even slight variations in basis sets can lead to widely different results [18, 20, 23], and greater proximity to experimental values has often been obtained from smaller basis sets [18, 20, 24]. The varied applications of the dilated electron propagator have established its usefulness but no attempt has been made to systematically explore the role of basis set variations on resonance attributes.

It is our purpose in this article to investigate the basis set dependence of resonance energies and widths of the prototypical ^{2}P shape resonances in e–Be and e–Mg scattering using the biorthogonal dilated electron propagator method. Towards this end, we examine the resonant attributes of the ^{2}P Be$^-$ and ^{2}P Mg$^-$ shape resonances calculated from the second-order decoupling of the dilated electron propagator using systematically constructed basis sets for Be and Mg. A correlation between the radial probability density profile of the resonant Feynman–Dyson amplitudes (FDAs) from different primitive bases and their impact on the resonance attributes is the chosen instrument for eliciting the role of basis set effects in the characterization of resonances. The results from different decouplings employing saturated basis sets for both the ^{2}P Be$^-$ and ^{2}P Mg$^-$ shape resonances are analyzed to decipher the role of relaxation and correlation in the characterization of these resonances.

The rest of the article is organised as follows. The main equations are collected in Sect. 2. The de-

Correspondence to: M. K. Mishra

tailed investigation of basis set effects on the resonant attributes in e–Be and e–Mg scattering is presented in Sect. 3 and a summary of the salient results concludes this article.

2 Method

The electron propagator technique [4, 6] is well established and the Dyson equation for the dilated biorthogonal matrix electron propagator, $\mathbf{G}(\eta, E)$, may be expressed as [14]

$$\mathbf{G}^{-1}(\eta, E) = \mathbf{G}_0^{-1}(\eta, E) - \mathbf{\Sigma}(\eta, E) \ , \tag{1}$$

where $\mathbf{G}_0(\eta, E)$ is the zeroth-order propagator for the uncorrelated electron motion, here chosen as given by the bivariational SCF approximation [17]. The self-energy matrix, $\mathbf{\Sigma}(\eta, E)$, incorporates the relaxation and correlation effects.

Solution of the bivariational SCF equations for the N-electron ground state yields a set of occupied and unoccupied spin orbitals. In terms of these spin orbitals, the matrix elements of $\mathbf{G}_0^{-1}(\eta, E)$ are

$$\left[\mathbf{G}_0^{-1}(\eta, E)\right]_{ij} = (E - \epsilon_i)\delta_{ij} \ , \tag{2}$$

where ϵ_i is the orbital energy corresponding to the ith spin orbital. Through the second order of electron interaction, the elements of the self-energy matrix are [14]

$$\Sigma_{ij}^2(\eta, E) = \frac{1}{2}\sum_{k,l,m} N_{klm} \frac{\langle ik \| lm \rangle \langle lm \| jk \rangle}{(E + \epsilon_k - \epsilon_l - \epsilon_m)} \ , \tag{3}$$

where

$$N_{klm} = (\langle n_k \rangle - \langle n_l \rangle)(\langle n_k \rangle - \langle n_m \rangle) \ , \tag{4}$$

with $\langle n_k \rangle$ being the occupation number (0 or 1) for the kth spin orbital and the anti-symmetric two-electron integral

$$\langle ij \| kl \rangle = \eta^{-1} \int \psi_i(1)\psi_j(2)[(1 - P_{12})/r_{12}]\psi_k(1)\psi_l(2)\mathrm{d}x_1\,\mathrm{d}x_2 \ . \tag{5}$$

The lack of complex conjugation stems from the biorthogonal sets of orbitals resulting from bivariational SCF being the complex conjugate of each other [12, 17]. For the diagonal 2ph-TDA [4, 6] decoupling of the dilated electron propagator [18]

$$\Sigma_{ij}^{\text{2ph-TDA}}(\eta, E) = \frac{1}{2}\sum_{k,l,m} N_{klm} \frac{\langle ik \| lm \rangle \langle lm \| jk \rangle}{(E + \epsilon_k - \epsilon_l - \epsilon_m) - \Delta} \ , \tag{6}$$

where

$$\begin{aligned} \Delta = {} & \tfrac{1}{2}\langle ml \| ml \rangle (1 - \langle n_m \rangle - \langle n_l \rangle) \\ & - \langle km \| km \rangle (\langle n_k \rangle - \langle n_m \rangle) - \langle kl \| kl \rangle (\langle n_k \rangle - \langle n_l \rangle) \ . \end{aligned} \tag{7}$$

In terms of the spin orbitals from the bivariational SCF procedure, combining Eqs. (1) and (2) we may write the matrix electron propagator as

$$\mathbf{G}^{-1}(\eta, E) = E\mathbf{1} - \boldsymbol{\epsilon}(\eta) - \mathbf{\Sigma}(\eta, E) \equiv E\mathbf{1} - \mathbf{L}(\eta, E) \tag{8}$$

or in operator form

$$G(\eta, E) = [E - L(\eta, E)]^{-1} \ , \tag{9}$$

whereby in terms of the eigenfunctions and eigenvalues of $L(\eta, E)$

$$L(\eta, E)\chi_n(\eta, E) = \mathscr{E}_n(\eta, E)\chi_n(\eta, E) \ . \tag{10}$$

The spectral representation of G is given by

$$G(\eta, E) = [E - L(\eta, E)]^{-1} \sum_n |\chi_n\rangle\langle\chi_n| = \sum_n \frac{|\chi_n\rangle\langle\chi_n|}{E - \mathscr{E}_n(\eta, E)} \tag{11}$$

and the eigenvalues of L, therefore, represent the poles of G. Accordingly, the dilated electron propagator calculations proceed by iterative diagonalization

$$\mathbf{L}(\eta, E)\chi_n(\eta, E) = \mathscr{E}_n(\eta, E)\chi_n(\eta, E) \ , \tag{12}$$

with

$$\mathbf{L}(\eta, E) = \boldsymbol{\epsilon}(\eta) + \mathbf{\Sigma}(\eta, E) \ , \tag{13}$$

where $\boldsymbol{\epsilon}(\eta)$ is the diagonal matrix of orbital energies and $\mathbf{\Sigma}$ is the self-energy matrix. The propagator pole, $\mathscr{E}$, is obtained by repeated diagonalizations such that one of the eigenvalues $\mathscr{E}_n(\eta, E)$ of $\mathbf{L}(\eta, E)$ fulfills the condition $E = \mathscr{E}_n(\eta, E)$ [14]. These $\mathscr{E}_n(\eta, E)$ represent the poles of the dilated electron propagator, $G(\eta, E)$. From among these poles, the resonant pole $\mathscr{E}_\mathrm{r}(\eta, E)$ and the corresponding eigenvector (FDA) $\chi_\mathrm{r}(\eta, E)$ are selected as per the prescription of the complex scaling theorems [8, 9], whereby those roots in the continua which are invariant to changes in the complex scaling parameter, η, are to be associated with resonances. In a limited basis set calculation, instead of absolute stability one finds quasistability where the θ trajectory displays kinks, cusps, loops or inflections which indicate the proximity of a stationary point [28]. In this work the resonance attributes were extracted from the value at the kink in the θ trajectories ($\partial\mathscr{E}_\mathrm{r}/\partial\theta = 0$). The real part of the resonant pole furnishes the energy and the imaginary part the half width of the resonance.

The quasiparticle approximation [29] for a dilated electron propagator [24] results from a diagonal approximation to the self-energy matrix, with poles of the dilated electron propagator given by

$$E(\eta) = \epsilon_i + \Sigma_{ii}(\eta, E) \ , \tag{14}$$

which are determined iteratively beginning with $E = \epsilon_i$ and Σ_{ii} may correspond to any pertubative (Σ^2) or renormalized decoupling such as the diagonal $\Sigma^{\text{2ph-TDA}}$.

In the bivariationally obtained biorthogonal orbital basis $\{\psi_i\}$, the FDA χ_n is a linear combination

$$\chi_n(\vec{r}) = \sum_i C_{in}\psi_i(\vec{r}) \ , \tag{15}$$

where the mixing of the canonical orbitals allows the incorporation of relaxation effects and nondiagonal correlation effects. In the zeroth-order ($\mathbf{\Sigma} = 0$) and the quasiparticle approximations (diagonal $\mathbf{\Sigma}$), there is no mixing. The difference between the perturbative second-order (Σ^2) or renormalized diagonal 2ph-TDA ($\Sigma^{\text{2ph-TDA}}$) decouplings manifests itself through differences between the mixing coefficients, C_{in}, from these approximations.

3 Results and discussion

The ^{2}P Be$^-$ [11, 18, 30–34] and the ^{2}PMg$^-$ [18, 30, 31, 36–39] shape resonances have been popular prototypical systems for testing new schemes for the treatment of electron-scattering resonances. Characterization of resonances using complex scaling ($\eta = \alpha e^{i\theta}$) requires that, once uncovered, resonant poles be stable with respect to further variations in the complex scaling parameter [8, 9]. In a limited basis set calculation, only quasistability in a narrow range of α and θ values is seen [28] and the resonances are identified by plotting the complex poles as a function of θ (θ trajectory) and associating the value of the resonant pole at the inflection point (θ_opt) in the quasistable region of this θ trajectory with the resonance energy (the real part) and half width (the imaginary part). Due to the need to ascertain stability with respect to variations in η, the dilated electron propagator calculations require θ and α trajectories necessitating sampling of about 20–25 θ values and 3–5 α values, making them computationally demanding. The previous dilated electron propagator calculations have therefore employed modest basis sets (10s6p) [11, 18], (5s7p) [11]

for Be^- and (4s7p, 4s8p, 4s9p and 4s10p) [18, 20, 21] for Mg^- shape resonances. In this work we chose to study the Be^- resonance by using the largest (14s16p) basis set [32] utilized for this system because this basis set gives a good coverage in the *s* space and the *p* space. The last five s-type functions differ by a factor of 2 in their exponents, while all the p-type functions differ by a factor of 2.26. The most diffuse s function has an exponent of 0.0032 and the most diffuse p function has an exponent of 0.0000334. Inadvertently, the p exponents used here are given by $15.46/2.26^n$ for $n = 1, \ldots, 16$, whereas in Ref. [32] $n = 0, \ldots, 15$. We checked our results with the $n = 0, \ldots, 15$ p basis set as well and found the difference between results from the 14s16p basis employed in this work and that used in Ref. [32] to be negligible. As a crude test for effects of *d* orbitals we augmented the basis set with a typical d polarization function [$\alpha(\mathrm{d}) = 4.0$] as well [40].

The ^{2}P Mg^- shape resonance is well characterized experimentally [37] and the dilated electron propagator results from the 4s9p basis [18] are almost identical to those observed experimentally. For the ^{2}P Mg^- shape resonance we therefore utilized this 4s9p basis with systematic augmentation with additional s- and p-type functions. In the following subsections we present our results for the ^{2}P Be^- and ^{2}P Mg^- shape resonances. Among the many decouplings employed in the previous dilated electron propagator calculations, the second-order decoupling has provided balanced results [14] and our investigation of basis set adequacy is through the use of this decoupling. We do not expect computationally more expensive correlation methods to exhibit significant new basis set requirements to describe the resonance; however, a more advanced method may require additional basis functions to describe the reference wave function.

The smallest primitive basis set with results close to the biggest basis set was used in resonance calculations employing other decouplings. The difference between resonance attributes from different decouplings and the correlation of these differences with those mirrored by the radial density profiles are used to decipher the role of correlation and relaxation effects in the formation and decay of resonances.

3.1 The ^2P Be^- shape resonance

Resonant θ trajectories from the second-order decoupling employing the 14s16p1d and other basis sets obtained from it by systematic deletion of most diffuse s, p and d functions are presented in Fig. 1. Resonance energies and widths extracted from the quasistable portion of the corresponding trajectories are collected in Table 1. The 14s16p1d is a saturated basis set for our calculations since results from the 14s11p – 14s16p1d basis sets are almost identical. The resonance energy and the width of the ^{2}P Be^- shape resonance from these 14s11p – 14s11p1d basis sets are indistinguishable within the limits of experimental accuracy and further investigations using quasiparticle and the diagonal 2ph-TDA decouplings were done with this more economical 14s11p basis which serves as our reference basis set in further discussions. These results are included in Table 2 along with those from other methods. The Be atom has large static correlation effects which cannot be described by second-order perturbation theory. It is thus necessary to use an approach, for example, multiconfigurational SCF (MCSCF), which can tackle the static correlation effects, to calculate accurate resonance energies and widths for Be. However, as argued previously, the second-order dilated electron propagator method is sufficiently accurate and since it permits an unequivocal identification of the target lowest unoccupied molecular orbital as a correlated resonant FDA [23] it is our chosen instrument for assessing the specific basis set requirements for describing the resonance FDA.

We proceed by pruning diffuse orbitals which have little importance for the Be reference wave function. The SCF and second-order Møller–Plesset (MP2) energies vary by less than 0.1 mhartree from the smallest 10s6p basis set to the 14s16p basis set and only the 14s16p1d basis set gives an additional energy lowering of 2.3 mhartree. Thus, the basis set effects we see all stem from the description of the resonance in the dilated electron propagator and not from insufficient description of the reference wave function used in the propagator calculations. As seen from Table 1, the resonance energies from the different basis sets obtained by systematic deletion in each step of the most diffuse function starting with the saturated 14s16p1d basis range from 0.48 eV for the 14s11p basis to 1.31 eV for the 10s6p basis. The widths vary from 0.32 eV for the 10s8p basis to 1.59 eV for the 10s6p basis. The basis set effects are thus large indeed and the need for understanding basis set requirements for converged resonance energies and widths in dilated electron propagator calculations becomes obvious. To understand the role of primitive basis set variations we have therefore plotted in Fig. 2 the radial probability densities from the basis sets tested.

The effects of systematic pruning of the most diffuse *p* orbital in each step from 14s16p to 14s8p are shown in Figs. 1a and 2a. We note from Table 1 and Fig. 1a that with fewer than 11 *p* orbitals, the value for the width [$= 2\ \mathrm{Im}(E)$] quickly deteriorates. The most diffuse *p* function in the 14s10p basis set has an exponent of 0.0044476, corresponding to a value of $\sqrt{\langle p|r^2|p\rangle} \sim 17$ au. From Fig. 2a we see that for the 14s*n*p basis sets with $n \leq 10$ the radial density is qualitatively wrong for $r > 15$ au, it is thus clear that these basis sets are simply too compact to describe the density for $r > 15$ au. Combining this observation with the results in Table 1, we infer that the density for $r > 15$ au is important for a converged value of the width, and if the basis set cannot describe this density sufficiently well then it is moved to shorter distances, distorting the extent and lifetime of the metastable binding.

The effects of pruning the most diffuse *s* orbitals are shown in Figs. 1b and 2b. The effects shown here are clearly correlation effects, as the dilated SCF *p* orbital energies do not depend on the *s* orbitals (the SCF reference wave function is converged with the first ten *s* orbitals). As the MP2 energy is fairly insensitive to the pruning of these *s* orbitals we conclude that the diffuse

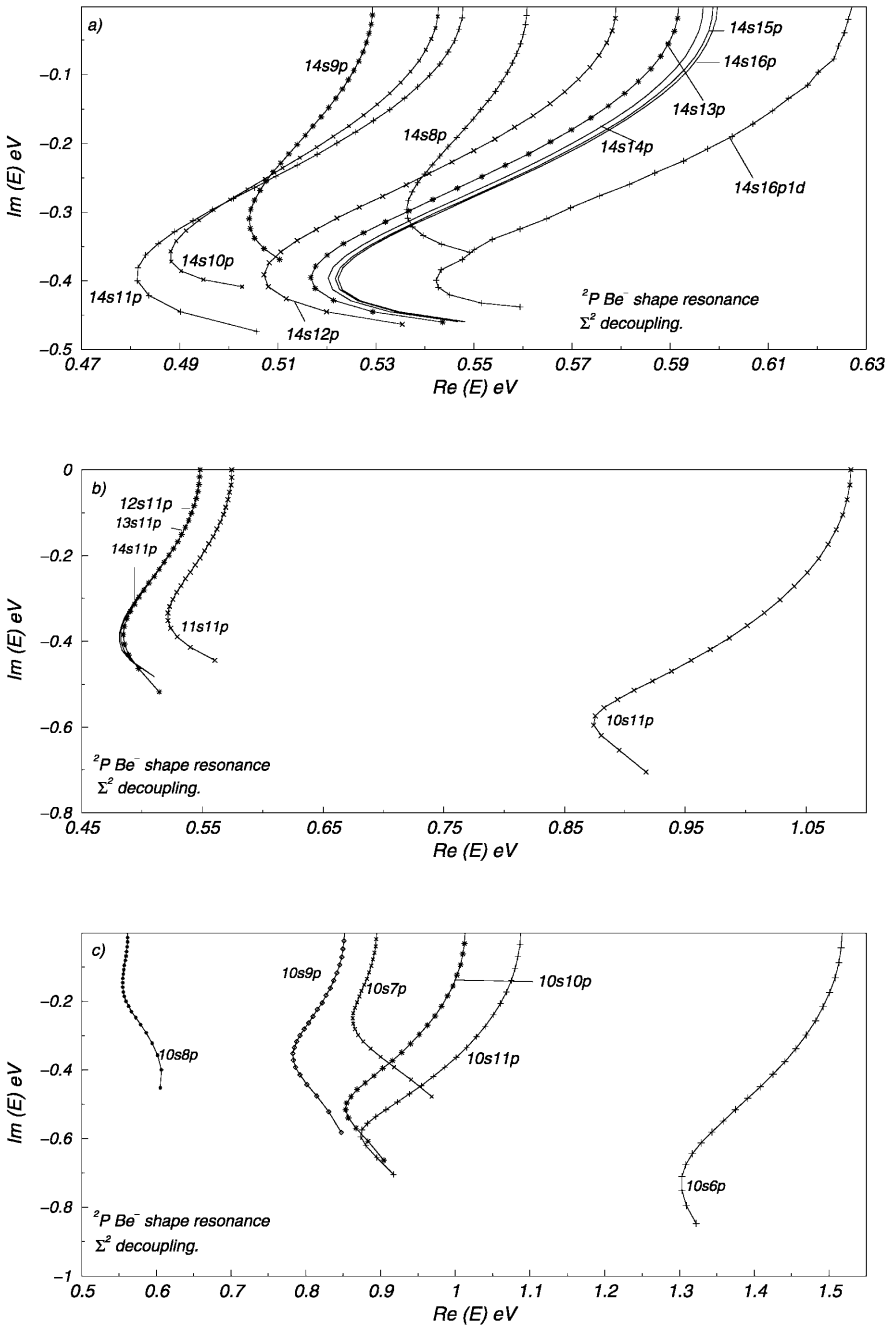

Fig. 1. θ trajectories from second-order decoupling of the dilated electron propagator for the ^{2}P Be$^-$ resonance using the Gaussian-type orbital (*GTO*) basis sets indicated in the figure. The complex scaling parameter $\eta = \alpha e^{i\theta}$, with $\theta = 0.0$ on the real line and θ increments in steps of 0.02 rad. The optimal α value for the 14s16p1d and 11s11p bases is 0.825 and for the rest is 0.8

s orbitals describe relaxation effects in the 2*s* orbital upon addition of the fifth electron. We note that there is a combination effect of the s space and the p space in the second-order calculations. The radial density is clearly too low for $r > 15$ au for the 10s11p basis set, while for 11s11p basis set the density is qualitatively correct. This is in confirmity with the calculated energies and widths given in Table 1. The most diffuse 11s basis function has an exponent of 0.026, corresponding to an expectation value of $\sqrt{\langle s|r^2|s\rangle} = 5.4$ au. As can be seen in Fig. 2b, there is a big fall in radial amplitude for $r < 5$ au from 10s11p and there is also a simultaneous reduction in the dip around $r = 8$ au. To confirm this assertion, we show in Figs. 1c and 2c the effect of basis set pruning all the way down to the 10s6p basis set. Figure 1c shows that the values vary a lot, and Fig. 2c illustrates how the removal of diffuse p functions forces the FDA to be more and more compact and consequently more and more different from the exact second-order solution. The radial density profile from the 10s6p basis is nodeless and mimics a compact 2*p*-type orbital, leading to the highest energy and width for resonance attributes coming from this basis.

As mentioned earlier, the resonance energies and widths obtained from the 14s11p – 14s16p1d basis sets are indistinguishable and we therefore employed the 14s11p basis set for the dilated electron propagator calculations using other decouplings. The resonant θ

Table 1. Second-order results for the ^{2}P shape resonance in e–Be scattering

Basis set	Energy (eV)	Width (eV)
14s/16p/1d	0.52	0.83
14s/16p	0.52	0.83
14s/15p	0.52	0.83
14s/14p	0.52	0.83
14s/13p	0.52	0.82
14s/12p	0.51	0.82
14s/11p	0.48	0.82
14s/10p	0.49	0.71
14s/9p	0.50	0.61
14s/8p	0.54	0.60
14s/11p	0.48	0.82
13s/11p	0.48	0.80
12s/11p	0.49	0.80
11s/11p	0.52	0.70
10s/11p	0.88	1.24
10s/11p	0.88	1.24
10s/10p	0.86	1.08
10s/9p	0.78	0.74
10s/8p	0.56	0.32
10s/7p	0.86	0.53
10s/6p	1.31	1.59

Table 2. Energy and width of the ^{2}P shape resonances in e–Be scattering

Method/reference	Energy (eV)	Width (eV)
Previous calculations		
Static exchange phase shift [30]	0.77	1.61
Static exchange plus polarizability phase shift [30]	0.20	0.28
Static exchange cross section [31]	1.20	2.6
Static exchange plus polarizability cross section [31]	0.16	0.14
Complex ΔSCF [32]	0.70	0.51
Singles doubles and triples complex configuration interaction [36]	0.32	0.30
S-matrix pole (X_α) [33, 34]	0.10	0.15
Exterior complex scaling [35]	0.11	0.10
Second-order dilated electron propagator based on real SCF [11]	0.57	0.99
Biorthogonal dilated electron propagator [18]	0.67	0.88
Second order [18]	0.64	0.60
Diagonal 2ph-TDA [18]	0.67	0.66
Present calculations (14s11p basis)		
Zeroth order	0.62	1.00
Second order	0.48	0.82
Quasiparticle second order	0.61	1.00
Diagonal 2ph-TDA	0.52	0.88
Quasiparticle diagonal 2ph-TDA	0.62	1.00

trajectories from the zeroth-order (first-order correction is zero), second-order, diagonal 2ph-TDA and their quaisparticle decouplings using the 14s11p basis set are plotted in Fig. 3a. The role of correlation is clearly seen. Correlation stabilizes and, thereby, lowers both the energy and the width. The second-order decoupling offers an energetically lower and sharper resonance compared to the resonance attributes obtained from the other decouplings. The resonance energies and widths from these different decouplings are collected in Table 2. The radial probability density differences between the second-order and zeroth-/first-order decouplings, and between the second-order and the diagonal 2ph-TDA decouplings are plotted in Fig. 3b. These plots show that Σ^2 and $\Sigma^{2ph\text{-}TDA}$ have similar radial density profiles, with Σ^2 bringing slightly higher electron density both near and far away from the nucleus in comparison to that from the $\Sigma^{2ph\text{-}TDA}$ decoupling and, thereby, lowering both the energy and the width. The $\Sigma^2 - \Sigma^0$ difference density plot shows that the correlation effects are indeed large and that the Σ^2 decoupling places much greater electron density in both large- and small-regions compared to the Σ^0 (SCF) approximation, whereby both the energy and the width are considerably lowered. This once more underscores the subtle and varied role of correlation effects in the formation and decay of resonances.

3.2 The ^2P Mg^- shape resonance

Resonant θ trajectories from the second-order decoupling employing different basis sets are presented in Fig. 4 and the resonance energies and widths extracted from the quasistable portion of the these trajectories are collected in Table 3. The resonance energies range from 0.09 eV for the 5s9p basis to 0.23 eV for the 8s13p basis and the widths range from 0.03 eV for the 5s9p basis to 0.13 eV for the 4s9p basis. Once again the basis set effects are quite large. The energy and width from the 4s9p basis are closest to the experimental results but the addition of a single s-type function leads to a change in resonance energy from 0.15 to 0.09 eV and a change in width from 0.13 to 0.03 eV for the 5s9p basis. Further augmentation with s-type functions alone makes little difference and the results show appreciable change only with the addition of extra p-type functions, with the resulting energy and width finally saturating for the 8s13p basis, and we take the 8s13p basis as the saturated basis for present calculations. In comparing this to the size of the saturated basis set used for Be one should remember that this basis set is contracted and that the Be sets are uncontracted. These results further emphasize the need for systematic augmentation of standard basis sets with sufficiently diffuse functions for converged resonance energies and widths. The energy and the width of the ^{2}P Mg^- shape resonance from the saturated 8s13p basis using different decouplings are included in Table 4. After saturating the diffuse p basis functions, we also returned to fill the gap in the core p basis three p functions with exponents 0.331, 0.165 and 0.082 between $\alpha(p) = 0.662$ and $\alpha(p) = 0.05$ of the 4s9p basis [20]. The addition of these core basis functions did not provide any appreciable change in energy or width and they are not discussed any further.

To understand the role of the basis set variations we have plotted the radial probability density profiles for the resonant root using the Σ^2 decoupling and some selected basis sets in Fig. 5. The 4s9p, 5s9p and 8s9p basis sets illustrate the effect of adding more diffuse s

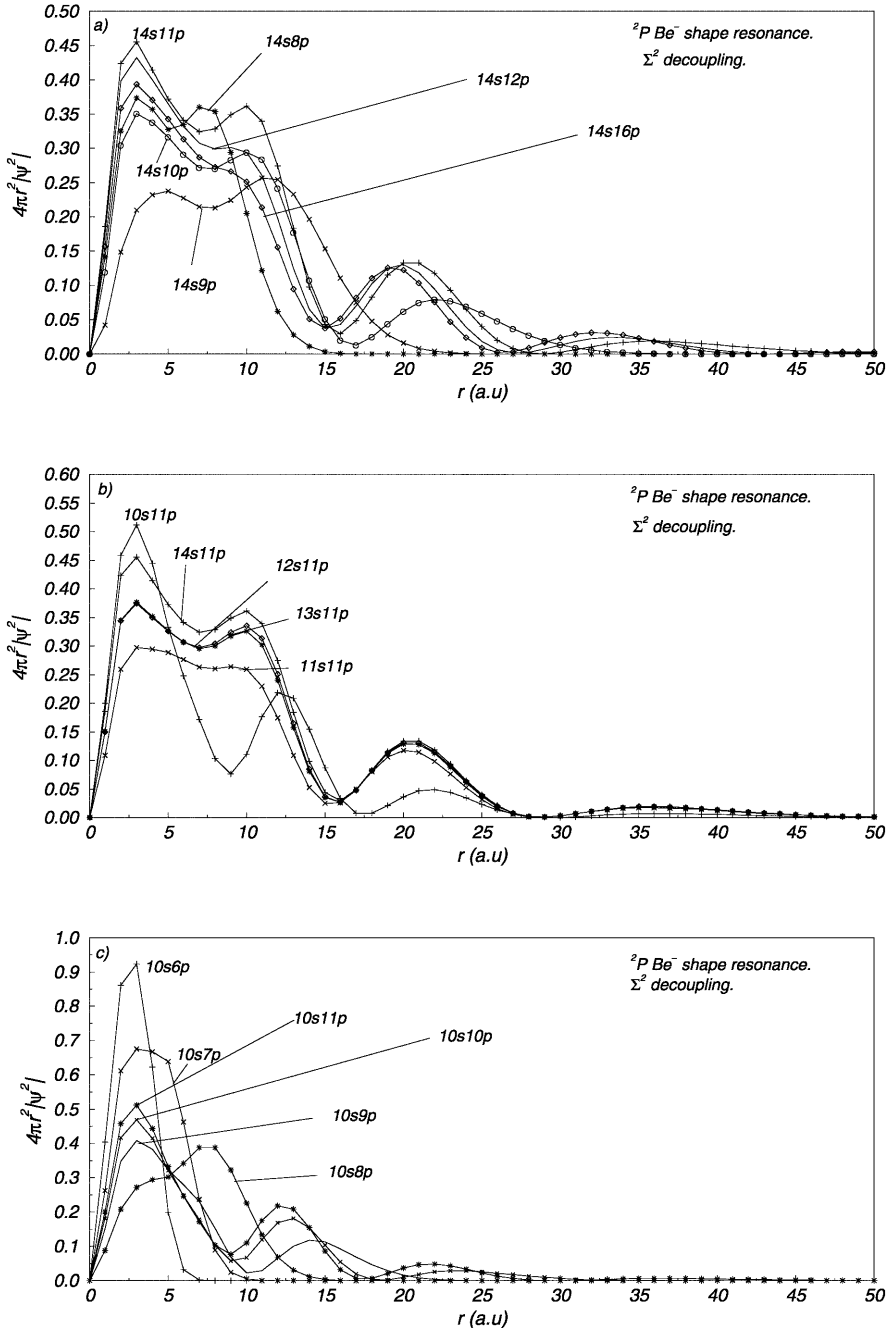

Fig. 2. Radial probability density for the ^{2}P Be$^-$ resonant Feynman–Dyson amplitudes (*FDA*) from the second-order decoupling using the basis sets indicated in the figure

functions, and the 8s9p, 8s11p and 8s13p basis sets illustrate the effect of adding more diffuse p functions. As Mg is a larger atom with a greater number of electrons, the densities peak at larger r values compared to those for Be. The radial probability density from the 4s9p basis is well distributed over a large area, with considerable density near the nucleus as well. In comparison, the radial density profile from the 5s9p basis has negligible electron density for $r < 20$ au, which minimizes interelectronic repulsion and leads to lower resonance energy and lesser instability manifesting itself as a smaller width cf. the arguments made earlier for e–Be scattering. The 8s9p curve resembles 4s9p for $r > 10$ au, but has no peak around 5 au and very little density for $r < 10$ au. The Hartree–Fock energies for the five basis sets vary by less than 0.002 hartree and we therefore conclude that the effect of s-basis functions is a correlation effect, as for Be. Apparently, the basis set deficiencies in s space lead to a competition between describing nodal structure and moving density away from small distances, and of the basis sets shown here only the basis sets with eight s functions are sufficiently flexible to describe both effects. We note that the energies and widths are very similar for 5s9p and 8s9p although the amplitudes are very different, showing that convergence cannot be assumed from close energy and width values alone. We also note that the three density amplitudes for 4s9p, 5s9p and 8s9p all are very similar

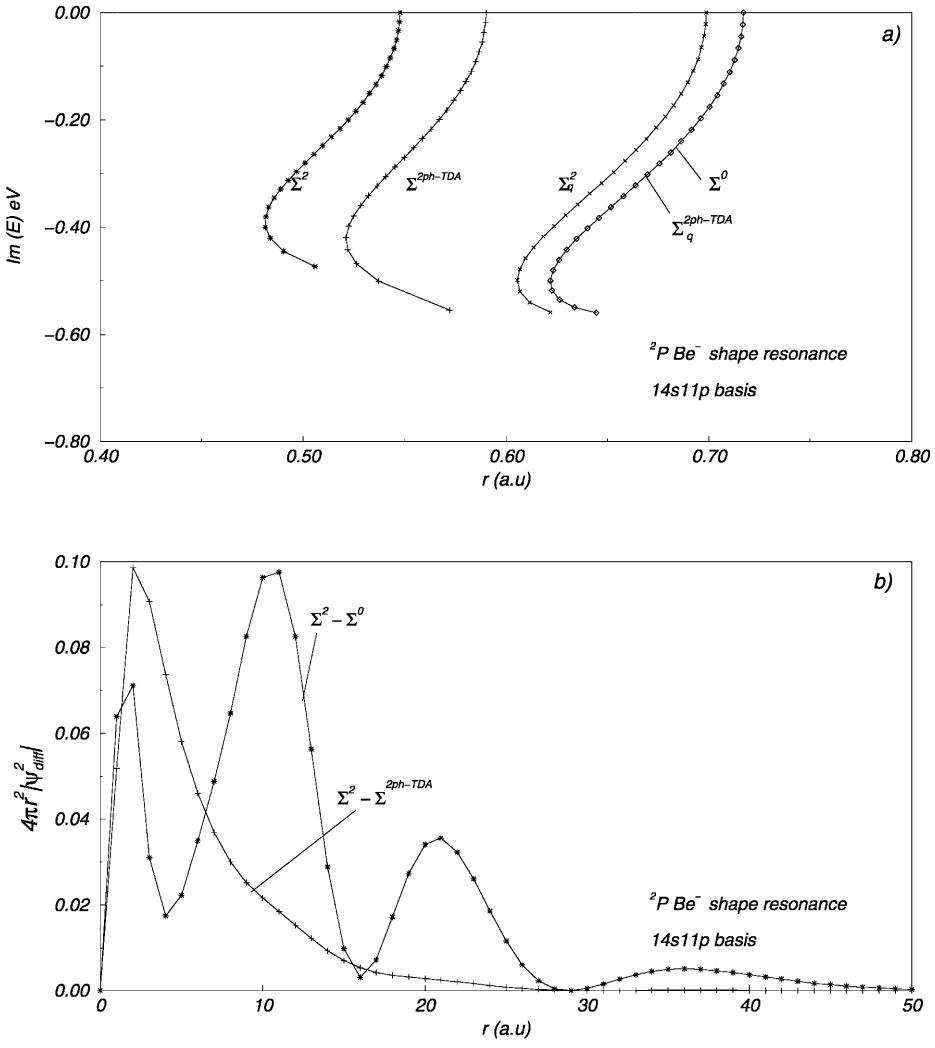

Fig. 3. **a** θ trajectories for the ^{2}P Be$^-$ resonant root from different decouplings using the 14s11p basis set. Conventions of Fig. 1 apply. The optimal α value is 0.8 for Σ^2, 0.825 for $\Sigma^{2ph\text{-}TDA}$, 0.9 for Σ_q^2 and 0.915 for $\Sigma_q^{2ph\text{-}TDA}$ and Σ^0 decouplings. **b** Difference in radial probability density obtained using the 14s11p basis set and Σ^2, Σ^0 and $\Sigma^{2ph\text{-}TDA}$ decouplings

$r > 40$ au. Adding more diffuse p functions to the 8s9p basis corrects this long distance density and nodal structure. For 8s11p, the node has moved from about 32 au to about 37 au. For 8s13p, this node stays at about 37 au but the basis is now sufficiently diffuse and flexible to describe another node at about 53 au. Furthermore, the 8s13p basis set has growing density at 60 au. The saturated 8s13p basis offers a balanced and well-distributed profile peaking at larger r compared to that from the 4s9p basis. It has small-r attributes similar to that of the 4s9p density but with no accumulation close to nucleus, whereby the resonance energy is higher. The width is lower because of lesser interelectronic repulsion. An intimate interplay between small-r and large-r behavior is once again seen to determine the resonance attributes, and as for Be we see that it is essential to include sufficiently diffuse functions in the basis set to describe the large-r density and a sufficient number of diffuse functions to describe the nodal structure.

The resonant θ trajectories from various decouplings of the dilated electron propagator using the saturated 8s13p basis are shown in Fig. 6. These results are collected in Table 4 and prove once more that basis set saturation is more important than incorporation of different decouplings. The results from all the decouplings are indistinguishable within the limits of experimental resolution. The radial probability density differences between the second-order and the diagonal 2ph-TDA decouplings and the second-order and the zeroth-order decouplings are plotted in Fig. 6b. The close proximity of the radial densities from all these decouplings explains the nearly similar results. The density profiles of Fig. 5, however, highlight the need for a better description of interelectronic repulsions and the incorporation of higher-order correlated decouplings therefore becomes most desirable.

4 Concluding remarks

The use of the dilated electron propagator method based on the bivariational SCF employing different primitive bases has shown that the description of resonances is extremely sensitive to the choice of primitive basis sets employed and that the effect of this sensitivity on the resonance attributes can be very large. The basis sets with a coordinate space span which can accomodate the competing pulls of providing accumulation of electron

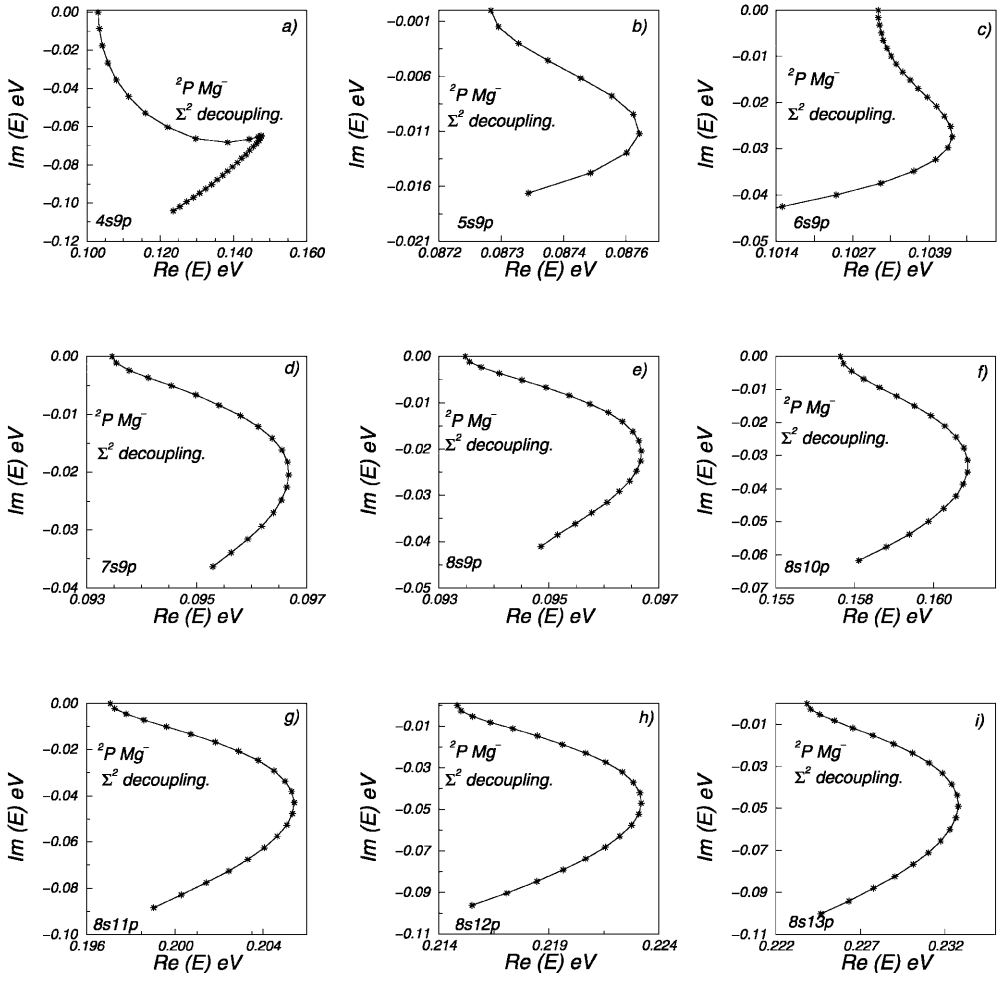

Fig. 4. θ trajectories from second-order decoupling of the dilated electron propagator using the contracted GTO bases 4s9p-8s9p (**a**–**e**) and the 8s10p-8s13p (**f**–**i**) bases. The conventions of Fig. 1 apply with $\theta = 0.0$ on the real line and θ increments in steps of 0.01 rad. The optimal α value is 0.75 for the 4s9p basis, 1.00 for the 5s9p basis, 1.05 for the 6s9p-8s9p bases, 1.02 for the 8s10p basis, 1.03 for the 8s11p basis and 1.025 for the 8s12p and 8s13p bases

Table 3. Second-order results for the ^{2}P shape resonance in e–Mg scattering

Basis set	Energy (eV)	Width (eV)
4s/9p	0.15	0.13
5s/9p	0.09	0.03
6s/9p	0.10	0.04
7s/9p	0.10	0.04
8s/9p	0.10	0.04
8s/10p	0.16	0.06
8s/11p	0.21	0.08
8s/12p	0.22	0.10
8s/13p	0.23	0.10

density near the nucleus to assist in resonance formation and also away from the nucleus to provide for its decay offer the most satisfactory results. A detailed investigation of basis set effects on resonance attributes was attempted for the first time and we studied the effects of ^{2}P Be^- and ^{2}P Mg^- shape resonances in some detail. The results offered here clearly indicate that the basis set saturation should precede the incorporation of higher-order decouplings. The diagonal 2ph-TDA decoupling sums the diagonal ring and ladder diagrams to all orders but does not offer any improvement over the second-

Table 4. Energy and width of the ^{2}P shape resonances in e–Mg scattering

Method/reference	Energy (eV)	Width (eV)
Experiment [37]	0.15	0.13
Previous calculations		
Static exchange phase shift [30/31]	0.46/0.46	1.37/1.53
Static exchange plus polarizability phase shift [30/31]	0.16/0.14	0.24/0.24
Static exchange cross section [31]	0.91	2.30
Static exchange plus polarizability cross section [31]	0.19	0.30
Configuration interaction [38]	0.20	0.23
S-matrix pole (X_α) [33, 34]	0.08	0.17
Exterior complex scaling [35]	0.15	0.13
Complex ΔSCF [39]	0.51	0.54
Dilated electron propagator based on real SCF [20]	0.14	0.13
Second order [18]	0.15	0.13
Diagonal 2ph-TDA [18]	0.15	0.13
Present calculations (8s13p basis)		
Zeroth order	0.25	0.10
Second order	0.23	0.10
Quasiparticle second order	0.24	0.10
Diagonal 2ph-TDA	0.24	0.10
Quasiparticle diagonal 2ph-TDA	0.24	0.10

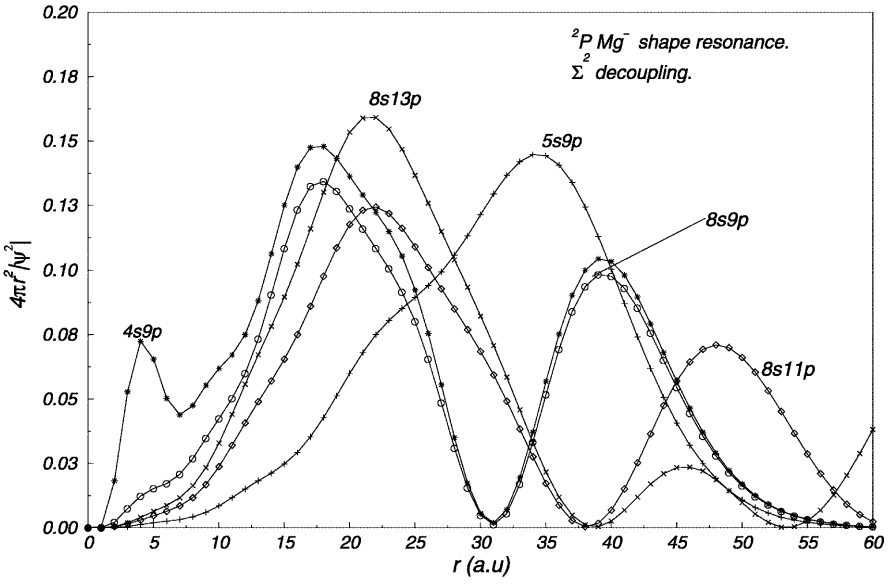

Fig. 5. Radial probability density plots for the ^{2}P Mg$^-$ resonant FDA from the second-order decoupling using 4s9p, 5s9p, 8s9p, 8s11p and 8s13p basis sets

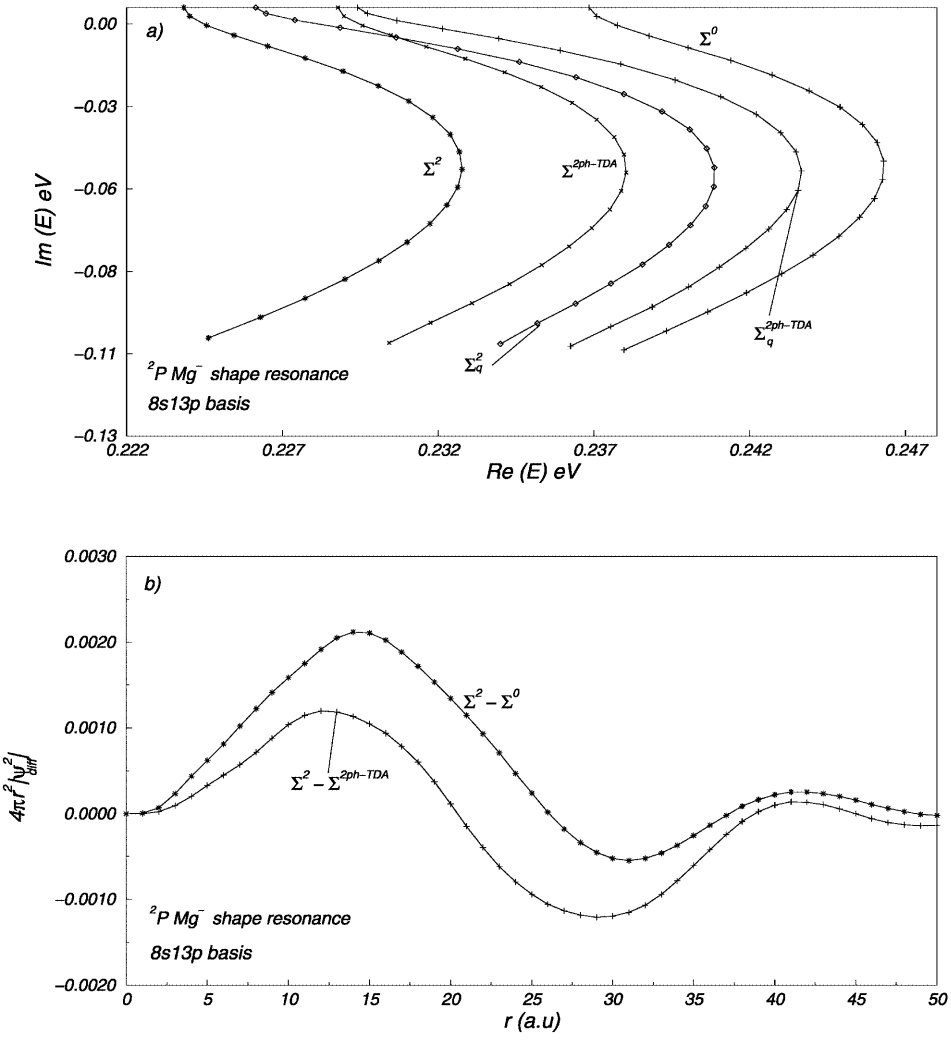

Fig. 6. **a** θ trajectories for the ^{2}P Be$^-$ resonant FDA from different decouplings using the 8s13p basis. The conventions of Fig. 4 apply. The optimal α value is 1.025 for Σ^2, 1.035 for $\Sigma^{2ph\text{-}TDA}$, 1.04 for Σ_q^2 and 1.045 for $\Sigma_q^{2ph\text{-}TDA}$ and Σ^0 decouplings. **b** Difference in radial probability density obtained using the 8s13p basis set and Σ^2, Σ^0 and $\Sigma^{2ph\text{-}TDA}$ decouplings

order results. As seen in the case of the e–Mg ^{2}P shape resonance, the results obtained with smaller bases may serendipitously match experimental results which vanish with basis set saturation. The present investigation, therefore, underscores the need for using saturated bases with sufficient flexibility to accumulate electron density

both close to and away from the nucleus and for higher-order decouplings such as the third-order and the partial fourth-order or MCSCF-type approaches to provide adequate incorporation of correlated interelectronic repulsions. Effort along these lines is underway in our group.

Acknowledgements. We are pleased to acknowledge financial support from the Department of Science and Technology, India (grant no. SP/S1/H26/96). A visit by M.K.M to Odense was supported by the Danish Natural Science Research Council (grant no. 9600856).

References

1. Linderburg J, Öhrn Y (1973) Propagators in quantum chemistry. Academic, New York
2. Jørgensen P, Simons J (1981) Second quantization based methods in quantum chemistry. Academic, New York
3. Cederbaum LS, Domcke W (1977) Adv Chem Phys 36: 205
4. Öhrn Y, Born G (1981) Adv Quantum Chem 13: 1
5. Herman MF, Freed KF, Yeager DL (1981) Adv Chem Phys 48: 1
6. von Niessen W, Schirmer J, Cederbaum LS (1984) Comput Phys Rep 1: 57
7. Ortiz JV (1992) Chem Phys Lett 199: 530
8. Reinhardt WP (1982) Annu Rev Phys Chem 33: 223
9. Junker BR (1982) Adv At Mol Phys 18: 207
10. Winkler P (1977) Z Phys A 291: 199
11. Donnelly RA, Simons J (1980) J Chem Phys 73: 2858
12. Mishra MK, Froelich P, Öhrn Y (1981) Chem Phys Lett 81: 339
13. Mishra MK (1989) In: Mukherjee D (ed) Lecture notes in quantum chemistry, vol 50. Springer, Berlin Heidelberg New York, p 223
14. Mishra MK, Medikeri MN (1996) Adv Quantum Chem 27: 223, and references therein
15. Mishra MK, Medikeri MN, Venkatnathan A, Mahalakshmi S (1998) Mol Phys 94: 127
16. Mishra MK, Öhrn Y, Froelich P (1981) Phys Lett A 81: 4
17. Löwdin PO, Froelich P, Mishra MK (1989) Adv Quantum Chem 20: 185
18. Medikeri MN, Nair J, Mishra MK (1993) J Chem Phys 99: 1869
19. Medikeri MN, Mishra MK (1994) J Chem Phys 100: 2044
20. Donnelly RA (1982) J Chem Phys 76: 5414
21. Mishra MK, Kurtz HA, Goscinski O, Öhrn Y (1983) J Chem Phys 79: 1896
22. Mishra MK, Goscinki O, Öhrn Y (1983) J Chem Phys 79: 5505
23. Medikeri MN, Mishra MK (1995) Chem Phys Lett 246: 26
24. Medikeri MN, Mishra MK (1993) Chem Phys Lett 211: 607
25. Mahalakshmi S, Mishra MK (1998) Chem Phys Lett 296: 43
26. Mahalakshmi S, Mishra MK (2000) Indian J Chem (in press)
27. Venkatnathan A, Mishra MK (1998) Chem Phys Lett 296: 223
28. Moiseyev N, Friedland S, Certain PR (1981) J Chem Phys 74: 4739
29. (a) Cederbaum LS (1975) J Phys B 8: 290; (b) Cederbaum LS Theor Chim Acta 31: 239
30. Kurtz HA, Öhrn Y (1979) Phys Rev A 19: 43
31. Kurtz HA, Jordan K (1981) J Phys B At Mol Opt Phys 14: 4361
32. McCurdy CW, Rescigno TN, Davidson ER, Lauderdale JG (1980) J Chem Phys 73: 3268
33. Krylstedt P, Rittby M, Elander N, Brändas EJ (1987) J Phys B At Mol Opt Phys 20: 1295
34. Krylstedt P, Elander N, Brändas EJ (1988) J Phys B At Mol Opt Phys 21: 3969
35. Krylstedt P, Elander N, Brändas EJ (1989) J Phys B At Mol Opt Phys 22: 1623
36. McCurdy CW, McNutt JF (1983) Chem Phys Lett 94: 306
37. Burrow PD, Michedja JA, Comer J (1976) J Phys B At Mol Opt Phys 9: 3255
38. Hazi AU (1978) J Phys B At Mol Opt Phys 11: L259
39. McCurdy CW, Lauderdale JG, Mowrey RC (1981) J Chem Phys 75: 1835
40. Kurtz HA, Elander N, Goscinski O, Sangfelt E (1981) Int J Quantum Chem Symp 15: 143